Biosensors and Bioelectronics 183 (2021) 113203

Contents lists available at ScienceDirect

Biosensors and Bioelectronics

journal homepage: http://www.elsevier.com/locate/bios

Amperometric aptasensor with sandwich-type architecture for troponin I based on carboxyethylsilanetriol-modified graphene oxide coated electrodes

Anabel Villalonga , Itziar Estabiel , Ana M. Pérez-Calabuig , Beatriz Mayol , Concepción Parrado , Reynaldo Villalonga *

Nanosensors and Nanomachines Group, Department of Analytical Chemistry, Faculty of Chemistry, Complutense University of Madrid, 28040, Madrid, Spain

ARTICLE INFO

Keywords:
Biosensor
Cardiac troponin I
Screen-printed electrode
Graphene
Aptamer

ABSTRACT

A novel amperometric aptasensor for the specific detection of cardiac troponin I (cTnI) was constructed by using screen-printed carbon electrodes coated with a carboxyethylsilanetriol-modified graphene oxide derivative as transduction element. This novel carboxylic acid-enriched nanomaterial allows easy and high load immobilization of the capture aptamer molecules on the electrode surface. The biosensing interface was assembled by covalent attachment of an amino-functionalized DNA aptamer on the carboxylic acid-enriched electrode surface. The sensing approach relies on the specific recognition of cTnI by the aptamer and further assembly of a sandwich-type architecture with a novel aptamer-peroxidase conjugate as signaling element. The aptasensor was employed to detect the cardiac biomarker in the broad range from 1.0 pg/mL to 1.0 μg/mL with a detection limit of 0.6 pg/mL. This electroanalytical device also showed high specificity, reproducibility and stability, and was useful to quantify cTnI in reconstituted human serum samples.

1. Introduction

Cardiovascular diseases constitute a major health problem with pandemic dimensions, being the first cause of mortality in the world (Roth et al., 2017). Among these diseases, myocardial infarction (MI) is the most common and deadliest form, representing over 15% of all global deaths (Jayaraj et al., 2018). Early diagnosis and systematic monitoring is the key to improve the survival rate for MI patients (Boeddinghaus et al., 2017). That is why, the development of portable and sensitive analytical methods for the prognosis and monitoring of MI biomarkers is a priority in clinical medicine.

Cardiac troponin testing has been the standard of practice for the diagnosis of MI, early rule-out, risk stratification, and outcomes assessment in patients presenting with acute coronary syndrome and non-acute coronary syndrome of myocardial injury (Twerenbold et al., 2017). In special, cardiac troponin I (cTnI) is considered the "gold standard" for MI diagnosis because this protein is quickly and specifically released to the blood circulation after a heart damage (Park et al., 2017). In addition to this extraordinary specificity for myocardial injury, the detection of this biomarker is highly sensitive for MI and even minimally elevated cTnI levels identify patients at increased risk for death and recurrent ischemic events.

During the last years, numerous affinity-based analytical assays have been developed for cTnI quantification by using colorimetric (Miao et al., 2019; Çimen et al., 2020; Zhou et al., 2018), electrochemical (Kazemi et al., 2016; Sun et al., 2019a, 2019b; Zhang et al., 2018; Wang et al., 2016; Negahdary et al., 2018; Jo et al., 2015; Yan et al., 2018; Shen et al., 2019; Lv et al., 2019), fluorescence (Lou et al., 2018; Wang et al., 2019) and chemiluminescence detection (Han and Kim, 2020). In this sense, antibodies has been the predominant biorecognition elements employed for these assays, and various immunological test for cTnI are currently in the market (Han et al., 2016). However, increased interest is currently devoted to use aptamers as affinity bioreceptors for cTnI detection, due to the high stability and specificity of these biomolecules. Aptamers and their chemically modified derivatives can be also prepared at large scale through conventional synthetic methods (Villalonga et al., 2020a).

In this context, special interest has been devoted to construct electrochemical aptasensors for cTnI due to the high sensitivity, low cost and ease of use of these devices (Kazemi et al., 2016; Sun et al., 2019a,

* Corresponding author.
E-mail address: rvillalonga@quim.ucm.es (R. Villalonga).

https://doi.org/10.1016/j.bios.2021.113203
Received 6 October 2020; Received in revised form 13 March 2021; Accepted 25 March 2021
Available online 29 March 2021

2019b; Zhang et al., 2018; Wang et al., 2016; Negahdary et al., 2018; Jo et al., 2015; Yan et al., 2018; Shen et al., 2019; Lv et al., 2019). Electrochemical biosensors and measurement instruments can be also miniaturized allowing potential design of portable and patient-oriented devices for at-home self-testing of clinical biomarkers (Da Silva et al., 2017). Possibility for self-testing is quite relevant for MI patients, because high survival rate can be achieved if changes in blood cTnI are early detected (Boeddinghaus et al., 2017).

Several strategies have been employed to construct electrochemical aptasensors for cTnI with improved analytical properties. Undoubtedly, the most successful approaches are based on the use of nanomaterials as transduction elements (Kazemi et al., 2016; Zhang et al., 2018; Yan et al., 2018; Shen et al., 2019), as well as the design of original methods for signal production and amplification (Zhang et al., 2018; Lv et al., 2019). This work describes the combined use of these two strategies to assemble an amperometric aptasensor for cTnI. This biosensor take advantages on the use of screen-printed carbon electrodes coated with a new carboxyethylsilanetriol-modified graphene oxide derivative as transduction element. This nanostructured electrode was then covalently functionalized with an anti-cTnI specific ssDNA aptamer as biomolecular receptor, able to capture the biomarker through affinity interactions. A sandwich-type arrangement was further assembled on the electrode surface by using a novel peroxidase-anti-cTnI aptamer bioconjugate as signaling element, allowing the amperometric detection of the cardiac biomarker after incubation with a mixture of hydroquinone and H_2O_2.

Carboxylic acid residues in GO have been largely employed as covalent immobilization points for biological receptors to construct electrochemical biosensors (Hernández et al., 2014; Omar et al., 2016; Niu et al., 2017). In addition, covalent functionalization of GO with chloroacetic acid and 6-aminohexanoic acid has been used to increase the load capacity of bioreceptors for biosensing purposes (Goud et al., 2017; Beheshti-Marnani et al., 2019). However, the preparation and use in biosensor technology of this novel carboxyethylsilanetriol-modified GO derivative has not been previously reported.

2. Materials and methods

2.1. Materials

Graphene oxide (GO) and screen-printed carbon electrodes were provided by Orion High Technologies S.L. (Spain). cTnI, horseradish peroxidase (HRP), human blood serum (S2257-5 ML), tris(2-carboxyethyl)phosphine hydrochloride (TCEP), N-hydroxysuccinimide (NHS), 1-ethyl-3-(3-dimethylaminopropyl)carbodiimide (EDAC) and anti-cTnI specific ssDNA aptamer modified with a primary amino group at the 5' end (Apt, 5′–NH_2–$(CH_2)_6$ – CGTGCAGTACGCCAACCTTTCTCATGCGCTGCCCCTCTTA) (Jo et al., 2015) were acquired from Sigma-Aldrich (USA). Carboxyethylsilanetriol disodium salt (25% in water) was provided by Gelest (USA). All other chemicals were of analytical grade.

2.2. Instruments and electrodes

Electrochemical experiments were performed with screen-printed carbon electrodes, consisting of a carbon working electrode (4.0 mm diameter), a carbon counter electrode and Ag/AgCl pseudo-reference electrode. Electrochemical measurements were carried out with a PalmSens 4 potentiostat (PalmSens BV, The Netherlands). High-resolution field emission scanning electron microscopy (FE-SEM) was performed with a JEOL JSM 7600F microscope (JEOL Ltd., Japan). Transmission electron microscopy (TEM) measurements were performed with a JEOL JEM-2100 microscope (JEOL Ltd., Japan). FT-IR spectra were recorded on a PerkinElmer Spectrum 400 Series spectrometer (PerkinElmer, USA). Spectrophotometric measurements were performed with an Ultrospec™ 8000 Dual Beam UV/VIS spectrophotometer (Biochrom, UK).

2.3. Preparation of carboxyethylsilanetriol-modified graphene oxide (CES-GO)

GO (260 mg) was dispersed in 150 mL of 10 mM sodium phosphate buffer, pH 7.5 by using an ultrasound bath, and 250 μL of 25% (w/w) aqueous carboxyethylsilanetriol solution were added. The mixture was stirred at room temperature during 12 h, and further centrifuged. The resulting solid was successively washed with 80% ethanol, absolute ethanol and diethyl ether. The CES-GO derivative was dried under N_2 atmosphere and kept in desiccator until use.

2.4. Preparation of aptamer-peroxidase conjugate (Apt-HRP)

To prepare the oxidized enzyme derivative, 2.0 mg HRP were dissolved in 2.0 mL of cold 50 mM sodium acetate buffer, pH 5.0, and 4.0 mg of m-$NaIO_4$ were added. The mixture was stirred at 4 °C under dark conditions during 1 h, and then 100 μL ethylene glycol were added. After 1 h under continuous stirring at 4 °C, the mixture was dialyzed *vs* cold 10 mM sodium phosphate buffer, pH 7.6, and concentrated to 1.0 mg/mL by using 30K Amicon Ultra-05 centrifugal filter devices (EMD Millipore Corporation, USA).

To prepare the active aptamer with hairpin conformation, a thermal denaturation and refolding process was performed (Villalonga et al., 2020b). Briefly, 500 μL of a 100 μM Apt solution in 10 mM sodium phosphate buffer, pH 7.6 containing 5 mM $MgCl_2$ was prepared, heated at 95 °C during 5 min, and further slowly cooled to room temperature. The aptamer solution was diluted with cold buffer to 50 μM final concentration, and 500 μL were mixed with 500 μL of 1.0 mg/mL oxidized HRP solution. The mixture was stirred at 4 °C in the dark during 30 min, and 100 μL of 10 mM $NaBH_3CN$ were added. After 4 h under continuous stirring, the mixture was dialyzed *vs* cold 100 mM sodium phosphate buffer, pH 7.6 containing 5 mM $MgCl_2$ by using 30K Amicon Ultra-05 centrifugal filter devices. The Apt-HRP conjugate was diluted with the same buffer to 10 μM final concentration, and kept in refrigerator until use.

2.5. Preparation of aptamer-functionalized electrode (Apt-CES-GO/SPE)

To prepare the nanostructured electrode, 8.0 μL of 3.0 μg/mL CES-GO aqueous dispersion were dropped on the working electrode surface and let to dry. The electrode was washed with MilliQ water, dried under N_2 and then 8.0 μL of 100 mM sodium phosphate buffer, pH 6.0 containing 1.0 mg/mL EDAC and 1.0 mg/mL NHS were dropped on the working electrode surface. After 30 min incubation at 4 °C in a humid chamber, the electrode was washed with MilliQ water, dried under N_2, and then 8.0 μL of a 2.5 μM Apt solution in 100 mM sodium phosphate buffer, pH 7.6 containing 5 mM $MgCl_2$ were dropped on the working electrode surface. After 1 h incubation at 4 °C in a humid chamber, the electrode was washed with milliQ water to remove the unbound species, dried under N_2, and the working electrode was coated with 8.0 μL of 0.25 mM ethanolamine in 100 mM sodium phosphate buffer, pH 7.6. The electrode was incubated at 4 °C during 45 min, the washed and dried as previously described, and then 8.0 μL of a 5% casein solution (w/v) in 100 mM sodium phosphate buffer, pH 7.6 containing 5 mM $MgCl_2$ were dropped on the working electrode surface. After 1 h incubation at 4 °C in a humid chamber, the Apt-CES-GO/SPE electrode was washed with cold buffer, dried under N_2 and kept at 4 °C until use.

2.6. Analytical procedure

cTnI sample solution (8.0 μL), prepared in 100 mM sodium phosphate buffer, pH 7.6 containing 5 mM $MgCl_2$, were dropped on the working electrode surface and kept at room temperature during 30 min in a humid chamber. The electrode was then washed with cold buffer

and dried under N_2. The working electrode was then coated with 8.0 μL of a 10 μM Apt-HRP solution in 100 mM sodium phosphate buffer, pH 7.6 containing 5 mM $MgCl_2$, and incubated in a humidity chamber at 4 °C during 30 min. The electrode was then washed with cold buffer and dried under N_2. Further, 45 μL of a freshly prepared 10 mM hydroquinone (HQ) solution in 100 mM sodium phosphate buffer, pH 7.6, were transferred to the electrode surface and amperometric signals were recorded at −200 mV after addition of 5 μL of a freshly prepared 50 mM H_2O_2 solution.

3. Results and discussion

Scheme 1 schematizes the preparation of the chemically-modified GO derivative to be employed as transduction element, as well as the steps involved in assembly and analytical use of the electrochemical aptasensor for cTnI. GO has been largely exploited to construct catalytic and affinity electrochemical biosensors, due to the presence of functional chemical groups for the stable covalent immobilization of the biorecognition (Suvarnaphaet and Pechprasarn, 2017). Chemical modification of GO has been also used to produce derivatives with new and/or enriched functional groups allowing evaluation of alternative immobilization approaches and increasing the load capacity for bioreceptors (Chen et al., 2012).

Although silanization reactions has been previously used for GO modification for bioelectroanalytical purposes (Arenque et al., 2014; Araque et al., 2013; Boujakhrout et al., 2016), to our knowledge enrichment of this nanomaterial with additional carboxylic acid groups by covalent treatment with carboxyethylsilanetriol has not been reported. The synthetic approach here proposed to prepare the CES-GO derivative implies the covalent attachment of the carboxyethylsilanetriol moieties to the hydroxyl groups on the GO surface through a simple one-pot reaction (Scheme 1A). Such modification not significantly affected the morphology of the nanomaterial, although some wrinkled sheets were observed by TEM analysis (Fig. 1A and B and Fig. 1S in Supporting Information). Taking into account that chemical modification with carboxyethylsilanetriol should not cause intramolecular cross-linking in the GO sheets, we suppose such crumpled structures were folded during deposition of the nanomaterial on the TEM grill.

Modification of GO with the silane-coupling agent carboxyethylsilanetriol was confirmed by FT-IR spectroscopy, and the corresponding spectra for native and chemically modified GO are shown in Fig. 2C. Both nanomaterials exhibited absorption bands at 3400 cm^{-1}, 1727 cm^{-1}, 1610 cm^{-1}, 1220 cm^{-1} and 1050 cm^{-1} which can be ascribed to the $\upsilon_{O\text{-}H}$, $\upsilon_{C=O}$, $\upsilon_{C=C}$ + $\upsilon_{COO\text{-}(asymmetric)}$, $\upsilon_{C\text{-}O\text{-}O}$ and $\upsilon_{C\text{-}OH}$ stretching vibrations (Boujakhrout et al., 2015). In addition, the absorption band at 850 cm^{-1} can be associated to the bending vibration of the C=C groups in the graphene nanosheets. GO also exhibited the characteristics bending band for the hydroxyl groups at 1362 cm^{-1}, which disappeared after covalent modification of the nanomaterial surface with carboxyethylsilanetriol. It should be noticed that the increased ratio for the intensity of the ($\upsilon_{C=C}$ + $\upsilon_{COO\text{-}(asymmetric)}$)/$\upsilon_{C=O}$ bands around 1610 cm^{-1} and 1727 cm^{-1} could be associated to the introduction of new carboxylate groups after covalent modification of the nanomaterial. This fact was also supported by the appearence of a shoulder band at 1410 cm^{-1}, which can be ascribed to the symmetric stretching of the $-CO_2^-$ groups. The attachment of the carboxyethylsilanetriol moieties can be also confirmed by the small absorption bands around 2920 cm^{-1} – 2860 cm^{-1}, corresponding to the stretching vibration of $-CH_2$ groups in the silane derivative.

The thermal stability profile for the GO derivatives was studied by thermogravimetric analysis, and the corresponding thermograms are shown in Fig. 1D. Both nanomaterials displayed a first thermal transformation process in the range of 25–130 °C, corresponding to the removal of the adsorbed water molecules. A thermal decomposition was further observed, which can be ascribed to the degradation of the oxygen containing functional groups. However, covalent attachment of carboxyethylsilanetriol to the GO surface reduced the thermal stability of the resulting CES-GO derivative, by shifting the temperature for the maximum rate of weight loss from 224 °C to 183 °C. CES-GO also exhibited a second thermal decomposition process with a maximum rate of weight loss at 252 °C, probably associated with the oxidation of the aliphatic methylene groups from the carboxyethylsilanetriol moieties.

To assemble the aptasensor for cTnI, the electrode was first coated with the CES-GO derivative, as illustrated in Scheme 1B. The carboxylic

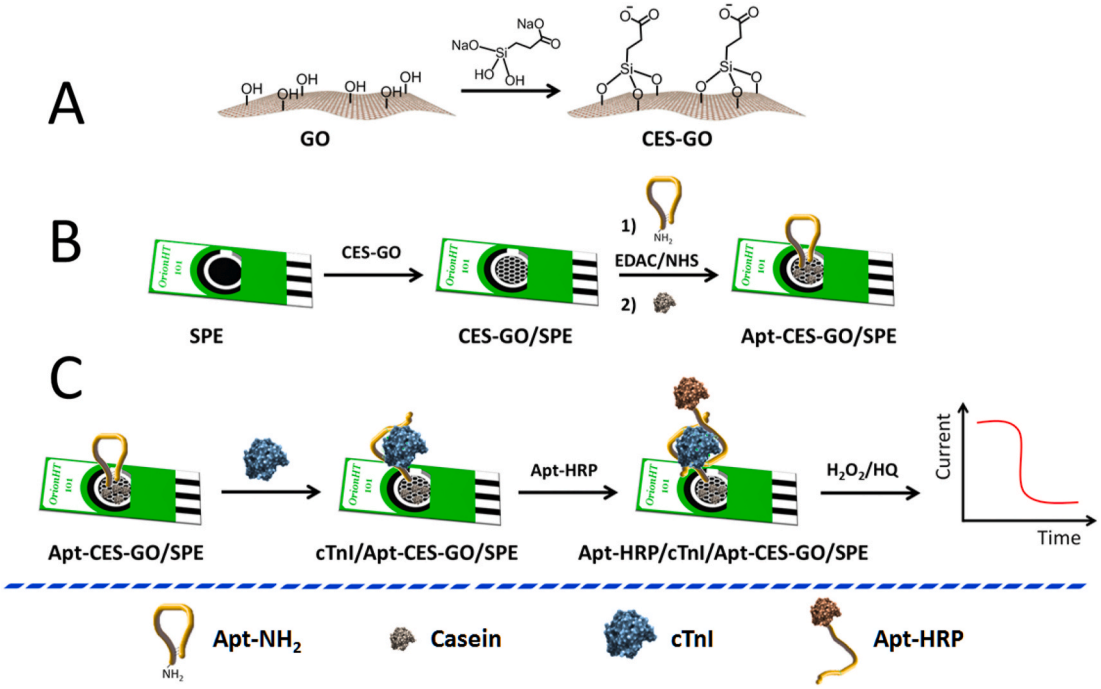

Scheme 1. Schematic display of the processes involved in the preparation of the CES-GO derivative (A) and the assembly (B) and method of use (C) of the aptasensor for cTnI.

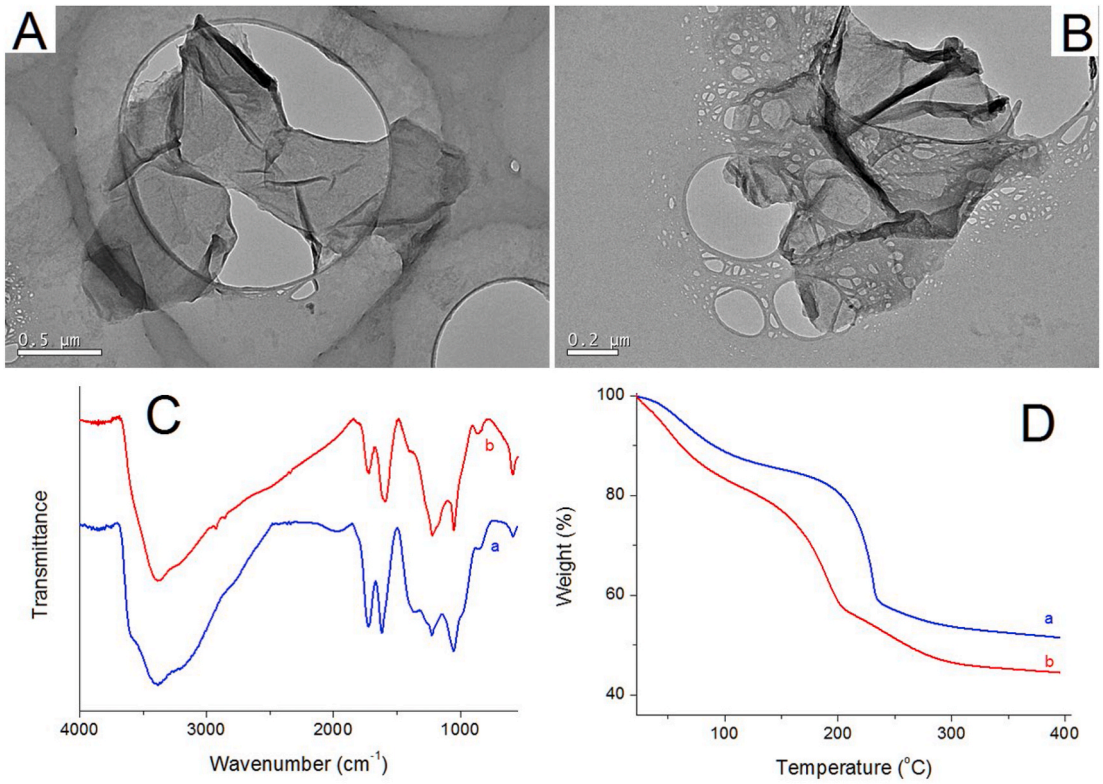

Fig. 1. Representative TEM images of GO (A) and CES-GO (B). FT-IR (C) and thermogravimetric analysis (D) for GO (a) and CES-GO (b).

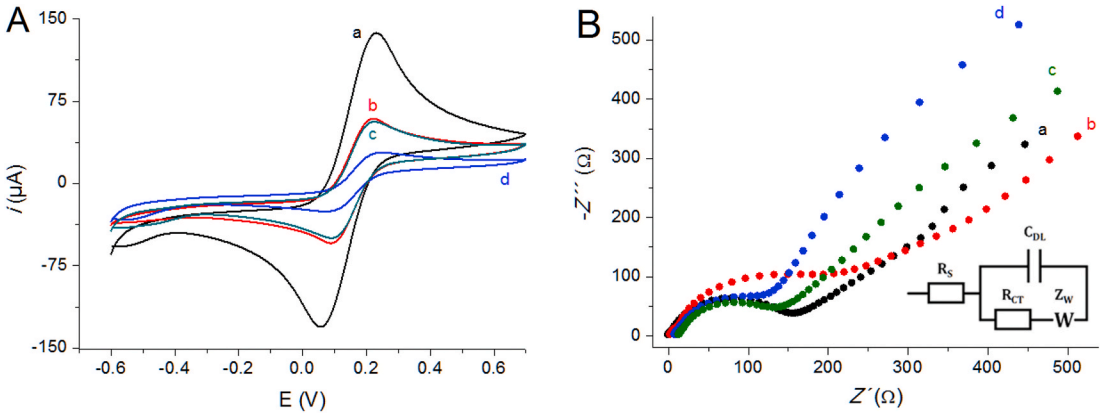

Fig. 2. Cyclic voltammograms (A, scan rate = 50 mV/s) and Nyquist plots (B) and of screen-printed carbon electrode before (a) and after sequential modification with CES-GO (b), Apt (c) and ethanolamine and casein (d), measured in 0.100 M KCl solution containing 5 mM $K_3[Fe(CN)_6]/K_4[Fe(CN)_6]$ (1:1). Inset in Fig. 2B: Randles equivalent circuit.

acid groups at the nanomaterial surface were further employed as linking points for the covalent immobilization of the specific ssDNA aptamer molecules modified with a primary amino group at the 5' end. This biofunctionalization process was performed by pre-activation of the carboxylic acid groups with NHS in the presence of EDAC, and further formation of covalent amide linkages with the aptamer molecules via a nucleophilic substitution reaction. Ethanolamine was further employed to modify the remained carboxylic acid groups at the electrode surface and milk casein was finally employed as blocking agent to reduce non-specific adsorptions of other sample components.

The capacity of the aptamer-functionalized electrode to quantify cTnI was assessed by using the methodology represented in Scheme 1C. This biosensing approach relies on the affinity-based recognition of the cardiac biomarker by the specific aptamer immobilized on the electrode surface and the further use of an aptamer-HRP conjugate as labelling element. Finally, the electroanalytical signal associated to the reduction of the enzymatically produced benzoquinone was measured by amperometry after addition of H_2O_2/hydroquinone to the sensor surface. At this point, it should be noticed that the specific activity of HRP was 4.4-fold reduced by chemical conjugation with the anti-cTnI ssDNA aptamer, as revealed by enzymatic assay.

The advantage of using CES-GO as transduction element was probed by comparing the analytical response of the aptasensor prepared as described in section 2.5 with those similarly assembled but using un-modified and GO-modified SPE as sensing interface. As can be observed in Fig. 2S (Supporting Information), higher electroanalytical signals were obtained from the Apt-CES-GO/SPE electrode, suggesting that the higher density of carboxylate groups at the nanostructured electrode

surface allows high load of immobilized aptamer, and accordingly, higher biorecognition capacity and biosensing response.

The construction of the electrochemical aptasensor was optimized by determining the effect of the different assembly steps on the amperometric response toward 100 pg/mL cTnI. Each optimization experiment was repeated three times, and the results are shown in Figs. 3S–7S (Supporting Information). Table 1 provides a summary of the studied and selected variables.

The assembling stages for the aptamer-functionalized electrode were characterized by different techniques. Fig. 8S in Supporting Information shows representative FE-SEM images of the electrode surface after sequential modification with the aptasensor components under the optimized conditions. Raw screen-printed electrode revealed a highly roughened surface composed by a 3D arrangement of carbon nanoparticles (Fig. 8S–A). Further coating with CES-GO was clearly evidenced by the presence of nanosheets of this material layered on the electrode surface (Fig. 8S–B). No significant differences in the electrode surface morphology was appreciated after functionalization with the aptamer (Fig. 8S–C), but a smoother surface was obtained after sequential modification with ethanolamine and coating with casein (Fig. 8S–D). Such effect could be justified by the non-conductive properties of the casein molecules used as blocking agent, affecting the resolution of the FE-SEM images.

Fig. 2A shows the cyclic voltammetric analysis of the raw and sequentially modified electrode, measured in 0.1 M KCl solution containing 5.0 mM $K_4[Fe(CN)_6]/K_3[Fe(CN)_6]$. A typical diffusion-limited cyclic voltammetric patterns was observed for SPE (curve a), CES-GO/SPE (curve b) and Apt-CES-GO/SPE (curve c) with ΔE values of 171 mV, 130 mV and 133 mV, and i_a/i_c values of 1.01, 1.02 and 1.05, respectively. According to these values, we can suggest a quasi-reversible behavior for the electron transfer process at these electrode surfaces. However, coating with CES-GO significantly decreased the intensity of the anodic and cathodic current peaks, and the electrochemical surface area of the electrode was reduced from 12.3 mm2 to 5.6 mm2 as determined according to the Randles-Sevcik model. This result suggests that CES-GO affected the electroconductive properties of the electrode surface. In addition, the negative charged carboxylate groups at the nanomaterial should produce electrostatic repulsion to the diffusion of the redox probe to the electrode interface.

Functionalization with the aptamer caused a little reduction in the intensity of the anodic and cathodic current peaks and the electrochemical surface area (5.4 mm2), probably associated to steric hindrance effects due to the attached DNA molecules. Although a higher reduction in these parameters could be expected, it should be taking into account that covalent immobilization of this bioreceptor reduced the density of carboxylate groups at the electrode surface, but this effect could be partially compensated by the introduction of the negative charged DNA aptamer molecules. In summary, the overall content of negative charged groups on the electrode surface could be similar for CES-GO/SPE and Apt-CES-GO/SPE electrodes. Further treatment with ethanolamine and coating with casein not significantly affected the quasi-reversible behavior for the electron transfer process at these electrode surfaces, with ΔE = 148 mV and i_a/i_c = 1.04 (curve d). However, a more drastic effect on the intensity of the anodic and cathodic current peaks and the electrochemical surface area (2.6 mm2) was appreciated, suggesting high coverage with these blocking agents.

Fig. 2B shows the Nyquist plots obtained by fitting the experimental data from electrochemical impedance spectroscopy to a conventional Randles equivalent circuit. The electron transfer resistance (R_{et}) for the screen-printed carbon electrode was increased from 183 Ω (curve a) to 229 Ω (curve b) and the Warburg element was reduced from 40.7° to 36.9°. These facts suggest the CES-GO derivative reduced the conductivity properties of the electrode surface thus affecting the occurrence of the electron transfer processes, and limited the diffusion of the negative charged electrochemical probe through electrostatic repulsions with the branched carboxylate groups. Further immobilization of the aptamer molecules caused a significant reduction in the electron transfer resistance (R_{et} = 161 Ω) but increased the Warburg element value to 61.2° (curve c), suggesting that mass transport of the redox probe is limited by the negative charged groups from the nanomaterial and the DNA bioreceptor. Finally, the electron transfer resistance increased (R_{et} = 186 Ω) after treatment the electrode with ethanolamine and casein (curve d), as expected due to the non-conductive properties of these blocking molecules. Covalent modification of the remaining carboxylate groups with ethanolamine and physical blocking with milk casein significantly reduced the electrostatic barrier effect on the electrode surface, as was noticed by the Warburg element value of 48.3°.

The aptamer-modified electrode was evaluated for the analytical determination of cTnI, and thus, the operational measurement conditions were optimized by using a 100 pg/mL solution of this biomarker. The results of these optimization experiments are shown in Table 1 and Figs. 9S–12S in Supporting Information. The ability of the immobilized aptamer to recognize cTnI and the further assembly of the affinity complex with the HRP-modified aptamer molecule were confirmed by cyclic voltammetry. As is illustrated in Fig. 13S in Supporting Information, less reversible behaviors for the electron transfer process at the electrode surface were observed after sequential incubation with the biomarker and the enzyme-modified aptamer, which was also associated with a significant reduction in the intensity of the anodic and cathodic current peaks. Changes in the cyclic voltammetric pattern of the electrode after incubation with Apt-HRP also suggests the formation of the sandwich-type biomolecular architecture proposed in Scheme 1.

To evaluate the effect of aptamer folding on the analytical response of the aptasensor, the amperometric signals of the Apt-CES-GO/SPE device toward 100 pg/mL cTnI in buffered solutions was compared with the corresponding to electrodes similarly prepared but using aptamer molecules without thermal unfolding and refolding treatments. We can expect that the proportion of folded aptamer molecules in this preparation will be lower than in those prepared by using the conventional folding protocol. As controls, electrodes assembled without aptamer and with anti-carcinoembriogenic antigen (anti-CEA) aptamer were used. As can be observed in Fig. 14S (Supporting Information), negligible amperometric responses were observed for the control electrodes after sequential incubation with cTnI and the Apt-HRP conjugate. On the contrary, high amperometric signals were recorded for the Apt-CES-GO/SPE aptasensor, which was 2.4-times higher than those from the electrode prepared with the unfolded anti-cTnI aptamer. These results confirm that the capture aptamer is still exposed after coating with casein and ethanolamine, mainly folded, and able to recognize cTnI.

The calibration plot in buffered solutions was further obtained under the optimized working conditions, and the result is shown in Fig. 3A. The amperometric aptasensor exhibited a fast response (Fig. 3B), and a linear relationship between amperometric signal and the logarithm of cTnI concentration between 1.0 pg/mL and 1.0 μg/mL according to the following equation (r^2 = 0.997, n = 10):

$$\Delta i_c(\mu A) = 0.93 \cdot \log[\text{cTnI}]\ (\text{pg/mL}) + 5.49$$

Table 1
Optimization of the experimental conditions for the assembly and use of the amperometric aptasensor for cTnI.

Variable	Range Tested	Selected Value
Amount of CES-GO (ng)	0–100	20
Apt concentration (μM)	0–20	2.5
Immobilization time for Apt (min)	30–210	60
Casein concentration (%, w/v)	0–10	5.0
Incubation time for casein (min)	25–90	60
Working pH	7.0–7.8	7.6
Incubation time for cTnI (min)	15–90	30
Apt-HRP concentration (μM)	0–15	10
Incubation time for Apt-HRP (min)	15–60	30

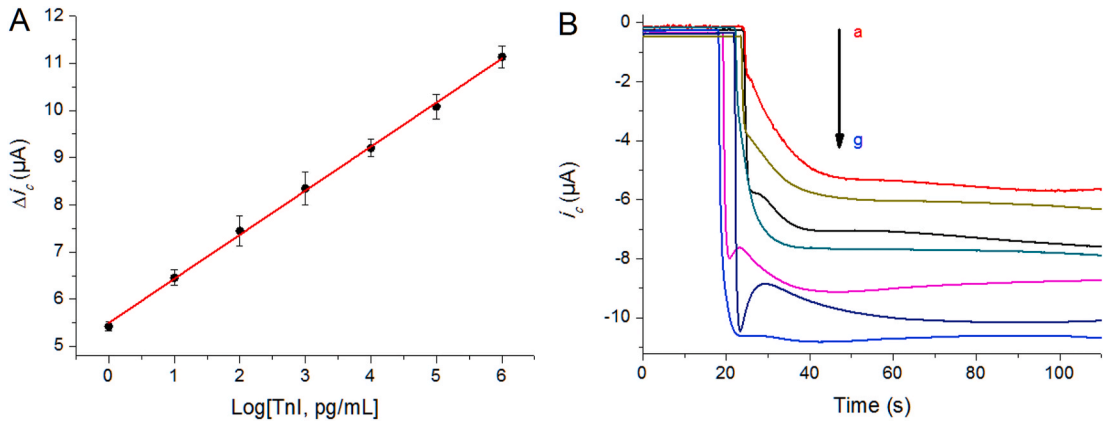

Fig. 3. Calibration plot (A) and representative amperograms (B) recorded with the aptasensor towards cTnI from 1.0 pg/mL (a) to 1.0 μg/mL (g) in buffered solutions.

The limit of detection for this aptasensor was estimated as 0.6 pg/mL, according to the IUPAC rules. This detection limit is lower than the 99th percentile cut-off value of 28 pg/mL established for cTnI with the commercial highly sensitive assay (Eggers et al., 2009). This electroanalytical device also showed good reproducibility, with a RSD = 12.3% as determined from ten different aptasensors toward 100 pg/mL cTnI in buffered solution.

The aptasensor showed a broad range of response and low limit of detection for cTnI, and these analytical properties were better or similar than those previously described for other electrochemical biosensors for this cardiac biomarker. As can be observed in Table 2, only two biosensors using antibodies as biorecognition element instead aptamers showed lower detection limits. In this sense, Zhang and collaborators constructed an electrochemical immunosensor able to detect up to 0.17 pg/mL cTnI by using gold nanoparticles-decorated polypyrrole-modified titanium dioxide nanoparticles as transduction element and gold nanoparticles doped covalent organic frameworks with toluidine blue as label for signal amplification (Zhang et al., 2018). In addition, Lv and co-workers reported a detection limit of 33 fg/mL for a sandwich-type immunosensor based on gold nanocubes functionalized graphene oxide as transduction interface and bimetallic gold/silver core-shell nanocubes and nitrogen and sulfur co-doped reduced graphene oxide as the signal amplifier (Lv et al., 2019). This immunosensor also showed a six-order range of response, which is similar to the present aptasensor device. In both cases, the complexity of the materials used for transduction and signal amplification was higher than those employed in the present work.

Table 2
Analytical properties of electrochemical biosensors for cTnI quantification.

Biosensor	Linear Range (pg/mL)	LOD (pg/mL)	Technique	Ref.
Ab/PrGO/GCE	100–10^4	70	EIS	Kazemi et al. (2016)
MCH/NTH-Tro4+Tro6/SPGE	50–10^5	16	DPV	Sun et al. (2019a)
BSA/Ab/TiO_2-PPy-AuNPs/GCE	0.5–10^4	0.17	SWV	Zhang et al. (2018)
MCH/peptide/AuNPs/GCE	15.5–1.55·10^3	3.4	EIS	Wang et al. (2016)
MCH/NTH-Tro4/SPGE	10–10^5	7.5	DPV	Sun et al. (2019b)
MCH/Apt/GDE	30–2·10^3	10	DPV	Negahdary et al. (2018)
MCH/Apt/WGE	24–2.4·10^5	24	SWV	Jo et al. (2015)
BSA/Ab/CIL-HCNTs/GCE	10–6·10^4	6	DPV	Yan et al. (2018)
BSA/Ab/Nf/DIL-HCNTs/GCE	50–3·10^4	30	DPV	Shen et al. (2019)
BSA/Ab/AuNC/GO/GCE	0.1–2.5·10^5	0.033	DPV	Lv et al. (2019)
Apt-CES-GO/SPE	1.0–10^6	0.6	AMP	This work

Ab: monoclonal antibody; PrGO: porous graphene oxide; GCE: glassy carbon electrode; MCH: 6-mercapto-1-hexanol; NTH-Tro4+Tro6: DNA nanotetrahedron capture aptamer + aptamer-based nanoprobe; SPGE: screen printed gold electrode; BSA: bovine serum albumin; TiO_2: titanium dioxide nanoparticles; PPy: polypyrrole; AuNPs: gold nanoparticles; NTH-Tro4: DNA nanotetrahedron capture aptamer; Apt: aptamer; GDE: gold disk electrode; WGE: working gold electrode; CIL: carboxyl-terminated ionic liquid; HCNTs: helical carbon nanotubes; DIL: dialdehyde-functionalized ionic liquid; AuNC: gold nanocubes; GO: graphene oxide; LOD: limit of detection; EIS: electrochemical impedance spectroscopy; DPV: differential pulse voltammetry; SWV: square wave voltammetry; AMP: amperometry.

To determine the selectivity properties of this aptasensor, the analytical response toward four different proteins commonly found in human serum was determined. As is illustrated in Fig. 4A, the average signal measured toward 2.0 μg/mL C-reactive protein, 50 ng/mL myoglobin, 8.0 ng/mL human serum albumin and 100 ng/mL human immunoglobulin G represented less than 20% of the signal corresponding to 100 pg/mL cTnI. These facts suggest that the aptamer used as capture and labeling elements is highly selective to cTnI, and this property was also well reflected to the constructed aptasensor. On the other hand, Fig. 3B shown the relative analytical response of the aptasensor toward cTnI alone and combined with these proteins. No significant difference was observed for the analytical signal measured for cTnI in the absence and the presence of these potential interfering proteins. Accordingly, we can conclude that these proteins caused low interference on the analytical determination of cTnI with the amperometric aptasensor. This electroanalytical device also showed good long-term stability, retaining more than 90% of the initial sensing capacity toward 100 pg/mL cTnI after 3 weeks of storage 4 °C in dry conditions (Fig. 15S in Supporting Information).

To evaluate the behavior of this device in a more real and complex media, reconstituted human serum was employed. To prepare the samples, commercial lyophilized human serum sample was reconstituted with 1 mL water and then 5-fold diluted in 100 mM sodium phosphate buffer, pH 7.4 containing 0.1% (w/v) casein. The calibration plot obtained by the standard addition method revealed a linear relationship between amperometric signal and the logarithm of cTnI concentration between 10 pg/mL and 1.0 μg/mL (Fig. 16S in Supporting Information). The experimental data were fitted to the following equation (r^2 = 0.984, n = 10):

$$\Delta i_c(\mu A) = 0.57 \cdot \log[\text{cTnI}]\ (\text{pg/mL}) + 0.61$$

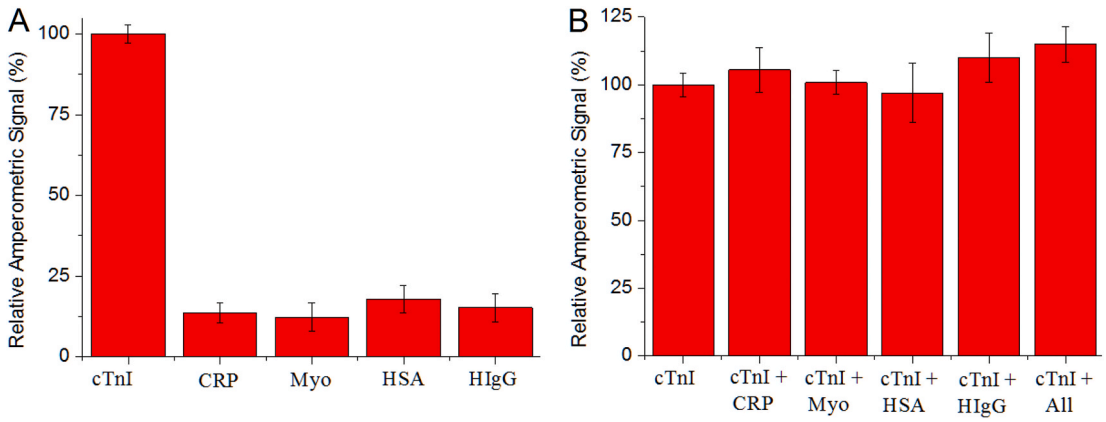

Fig. 4. A) Relative amperometric response of the aptasensor toward 100 pg/mL cTnI, C-reactive protein (CRP, 2.0 μg/mL), myoglobin (Myo, 50 ng/mL), human serum albumin (HSA, 8 ng/mL), and human immunoglobulin G (HIgG, 100 ng/mL). B) Response of the aptasensor toward cTnI and mixtures with other potential interfering proteins, at the same concentration cited above.

Different slope values for the calibration plots in buffer solution and reconstituted human serum revealed a matrix effect for this sample, and this effect was higher when undiluted serum samples were employed as expected. On the other hand, the detection limit estimated in human serum was higher (3.4 pg/mL) than those determined in buffer.

The aptasensor was validated for the quantification of cTnI in spiked human serum samples, by using the standard addition method. To do this, three different reconstituted human serum samples were spiked at 1.0 ng/mL cTnI and measured with the aptasensor. The average cTnI concentration in the spiked samples was estimated as (1.14 ± 0.08) ng/mL, representing a recovery of 114%. As a preliminary evaluation, the nanostructured sensor was also tested with a voluntary donor serum sample, and the results were compared with those obtained from the UniCel DxI 800 chemiluminescent immunoassay system by using the Access AccuTnI+3 assay. The average cTnI concentrations determined with the aptasensor and the chemiluminescent procedure were (5.1 ± 0.6) ng/L (n = 5) and (4.67 ± 0.03) ng/L (n = 3), respectively. The low relative error of 9.2% suggests high reliability and accuracy of this aptasensor for real sample analysis.

4. Conclusions

Here we reported the construction of an original amperometric aptasensor with sandwich architecture for cTnI determination. This device was assembled on disposable screen-printed carbon electrodes coated with a carboxyethylsilanetriol-modified graphene oxide derivative, which provided high density of carboxylic acid groups for the covalent attachment of the specific anti-cTnI DNA aptamer, and was prepared through a simple one-pot reaction. To generate an amplified analytical signal, a new aptamer-modified HRP conjugate was prepared and used as labeling element. The analytical performance of this biosensor was excellent, with a broad range of response, low detection limit, high reproducibility, specificity and stability. According to our results, we envision that this device could be used for the point-of-care detection of cTnI for early diagnosis of MI. In addition, the novel carboxylic acid-enriched GO derivative could be valuable for the construction of other catalytic and affinity biosensors with high load of covalently immobilized biological receptors (aptamers, antibodies, enzymes, nucleic acids, etc.). These carboxylic acid moieties can be also employed to anchor redox probes, nanoparticles, polymers and other materials on the GO surface to assemble electrochemical biosensors with improved analytical properties.

CRediT authorship contribution statement

Anabel Villalonga: Investigation, Validation, Supervision. **Itziar Estabiel:** Investigation. **Ana M. Pérez-Calabuig:** Investigation, Supervision. **Beatriz Mayol:** Investigation. **Concepción Parrado:** Supervision. **Reynaldo Villalonga:** Conceptualization, Methodology, Funding acquisition, Supervision, Writing – review & editing.

Declaration of competing interest

The authors declare that they have no known competing financial interests or personal relationships that could have appeared to influence the work reported in this paper.

Acknowledgements

Financial support from the Spanish Ministry of Economy and Competitiveness (project CTQ2017-87954-P) and the Comunidad de Madrid (Industrial PhD Program) is gratefully acknowledged.

Appendix A. Supplementary data

Supplementary data to this article can be found online at https://doi.org/10.1016/j.bios.2021.113203.

References

Araque, E., Villalonga, R., Gamella, M., Martinez-Ruiz, P., Reviejo, J., Pingarrón, J.M., 2013. J. Mater. Chem. B 1, 2289–2296.
Araque, E., Villalonga, R., Gamella, M., Martínez-Ruiz, P., Sánchez, A., García-Baonza, V., Pingarrón, J.M., 2014. ChemPlusChem 79, 1334.
Beheshti-Marnani, A., Hatefi-Mehrjardi, A., Es' haghi, Z., 2019. Colloids Surf. B Biointerfaces 175, 98–105.
Boeddinghaus, J., Reichlin, T., Nestelberger, T., Twerenbold, R., Meili, Y., Wildi, K., Hillinger, P., Giménez, M.R., Cupa, J., Schumacher, L., Schubera, M., 2017. Clin. Res. Cardiol. 106, 457–467.
Boujakhrout, A., Jimenez-Falcao, S., Martínez-Ruiz, P., Sánchez, A., Díez, P., Pingarrón, J.M., Villalonga, R., 2016. Analyst 141, 4162–4169.
Boujakhrout, A., Sánchez, A., Díez, P., Jiménez-Falcao, S., Martínez-Ruiz, P., Peña-Álvarez, M., Pingarrón, J.M., Villalonga, R., 2015. J. Mater. Chem. B 3, 3518–3524.
Chen, D., Feng, H., Li, J., 2012. Chem. Rev. 112, 6027–6053.
Çimen, D., Bereli, N., Günaydın, S., Denizli, A., 2020. Talanta 219, 121259.
Da Silva, E.T., Dênio, E.S., Barragan, J.T., Giarola, J. de F., de Moraes, A.C., Kubota, L.T., 2017. ChemElectroChem 4, 778–794.
Eggers, K.M., Jaffe, A.S., Lind, L., Venge, P., Lindahl, B., 2009. Clin. Chem. 55, 85–92.
Goud, K.Y., Hayat, A., Catanante, G., Satyanarayana, M., Gobi, K.V., Marty, J.L., 2017. Electrochim. Acta 244, 96–103.
Han, G.R., Kim, M.G., 2020. Sensors 20, 2593.
Han, X., Li, S., Peng, Z., Othman, A.M., Leblanc, R., 2016. ACS Sens. 1, 106–114.
Hernández, R., Vallés, C., Benito, A.M., Maser, W.K., Rius, F.X., Riu, J., 2014. Biosens. Bioelectron. 54, 553–557.
Jayaraj, J.C., Davatyan, K., Subramanian, S.S., Priya, J., 2018. In: Pamukçu, B. (Ed.), Intechopen.
Jo, H., Gu, H., Jeon, W., Youn, H., Her, J., Kim, S.K., Lee, J., Shin, J.H., Ban, C., 2015. Anal. Chem. 87, 9869–9875.
Kazemi, S.H., Ghodsi, E., Abdollahi, S., Nadri, S., 2016. Mater. Sci. Eng. C 69, 447–452.

Lou, D., Fan, L., Cui, Y., Zhu, Y., Gu, N., Zhang, Y., 2018. Anal. Chem. 90, 6502–6508.
Lv, H., Zhang, X., Li, Y., Ren, Y., Zhang, C., Wang, P., Xu, Z., Lin, X., Chen, Z., Dong, Y., 2019. Microchimica Acta 186, 416.
Miao, L., Jiao, L., Tang, Q., Li, H., Zhang, L., Wei, Q., 2019. Sensor. Actuator. B Chem. 288, 60–64.
Negahdary, M., Behjati-Ardakani, M., Sattarahmady, N., Heli, H., 2018. J. Biomed. Phys. Eng. 8, 167.
Niu, X., Zheng, W., Yin, C., Weng, W., Li, G., Sun, W., Men, Y., 2017. J. Electroanal. Chem. 806, 116–122.
Omar, M.N., Salleh, A.B., Lim, H.N., Tajudin, A.A., 2016. Anal. Biochem. 509, 135–141.
Park, K.C., Gaze, D.C., Collinson, P.O., Marber, M.S., 2017. Cardiovasc. Res. 113, 1708–1718.
Roth, G.A., Johnson, C., Abajobir, A., Abd-Allah, F., Abera, S.F., Abyu, G., Ahmed, M., Aksut, B., Alam, T., Alam, K., Alla, F., Alvis-Guzman, N., Amrock, S., Ansari, H., Ärnlöv, J., Asayesh, H., Atey, T.M., Avila-Burgos, L., Awasthi, A., Banerjee, A., Barac, A., Bärnighausen, T., Barregard, L., Bedi, N., Ketema, E.B., Bennett, D., Berhe, G., Bhutta, Z., Bitew, S., Carapetis, J., Carrero, J.J., Malta, D.C., Castañeda-Orjuela, C.A., Castillo-Rivas, J., Catalá-López, F., Choi, J.Y., Christensen, H., Cirillo, M., Cooper Jr., L., Criqui, M., Cundiff, D., Damasceno, A., Dandona, L., Dandona, R., Davletov, V., Dharmaratne, S., Dorairaj, P., Dubey, M., Ehrenkranz, R., Zaki, M.S., Faraon, E.J.A., Esteghamati, A., Farid, T., Farvid, M., Feigin, V., Ding, E. L., Fowkes, G., Gebrehiwot, T., Gillum, R., Gold, A., Gona, P., Gupta, R., Habtewold, T.D., Hafezi-Nejad, N., Hailu, T., Hailu, G.B., Hankey, G., Hassen, H.Y., Abate, K.H., Havmoeller, R., Hay, S.I., Horino, M., Hotez, P.J., Jacobsen, K., James, S., Javanbakht, M., Jeemon, P., John, D., Jonas, J., Kalkonde, Y., Karimkhani, C., Kasaeian, A., Khader, Y., Khan, A., Khang, Y.H., Khera, S., Khoja, A. T., Khubchandani, J., Kim, D., Kolte, D., Kosen, S., Krohn, K.J., Kumar, G.A., Kwan, G.F., Lal, D.K., Larsson, A., Linn, S., Lopez, A., Lotufo, P.A., Abd El Razek, H. M., Malekzadeh, R., Mazidi, M., Meier, T., Meles, K.G., Mensah, G., Meretoja, A., Mezgebe, H., Miller, T., Mirrakhimov, E., Mohammed, S., Moran, A.E., Musa, K.I., Narula, J., Neal, B., Ngalesoni, F., Nguyen, G., Obermeyer, C.M., Owolabi, M., Patton, G., Pedro, J., Qato, D., Qorbani, M., Rahimi, K., Rai, R.K., Rawaf, S., Ribeiro, A., Safiri, S., Salomon, J.A., Santos, I., Milicevic, M.S., Sartorius, B., Schutte, A., Sepanlou, S., Shaikh, M.A., Shin, M.J., Shishehbor, M., Shore, H., Santos Silva, D.A., Sobngwi, E., Stranges, S., Swaminathan, S., Tabarés-Seisdedos, R., Atnafu, N.T., Tesfay, F., Thakur, J.S., Thrift, A., Topor-Madry, R., Truelsen, T., Tyrovolas, S., Ukwaja, K.N., Uthman, O., Vasankari, T., Vlassov, V., Vollset, S.E., Wakayo, T., Watkins, D., Weintraub, R., Werdecker, A., Westerman, R., Wiysonge, C. S., Wolfe, C., Workicho, A., Xu, G., Yano, Y., Yip, P., Yonemoto, N., Younis, M., Yu, C., Vos, T., Naghavi, M., Murray, C., 2017. J. Am. Coll. Cardiol. 70, 1–25.
Shen, Q., Liu, M., Lü, Y., Zhang, D., Cheng, Z., Liu, Y., Gao, H., Jin, Z., 2019. ACS Omega 4, 11888–11892.
Sun, D., Lin, X., Lu, J., Wei, P., Luo, Z., Lu, X., Chen, Z., Zhang, L., 2019b. Biosens. Bioelectron. 142, 111578.
Sun, D., Luo, Z., Lu, J., Zhang, S., Che, T., Chen, Z., Zhang, L., 2019a. Biosens. Bioelectron. 134, 49–56.
Suvarnaphaet, P., Pechprasarn, S., 2017. Sensors 17, 2161.
Twerenbold, R., Boeddinghaus, J., Nestelberger, T., Wildi, K., Gimenez, M.R., Badertscher, P., Mueller, C., 2017. J. Am. Coll. Cardiol. 70, 996–1012.
Villalonga, A., Pérez-Calabuig, A.M., Villalonga, R., 2020a. Anal. Bioanal. Chem. 412, 55–72.
Villalonga, A., Vegas, B., Paniagua, G., Eguílaz, M., Mayol, B., Parrado, C., Rivas, G., Díez, P., Villalonga, R., 2020b. J. Electroanal. Chem. 877, 114511.
Wang, B., Jing, R., Qi, H., Gao, Q., Zhang, C., 2016. J. Electroanal. Chem. 781, 212–217.
Wang, X., Wang, X., Han, Y., Li, H., Kang, Q., Wang, P., Zhou, F., 2019. ACS Applied Nano Materials 2, 7170–7177.
Yan, H., Tang, X., Zhu, X., Zeng, Y., Lu, X., Yin, Z., Lu, Y., Yang, Y., Li, L., 2018. Sensor. Actuator. B Chem. 277, 234–240.
Zhang, T., Ma, N., Ali, A., Wei, Q., Wu, D., Ren, X., 2018. Biosens. Bioelectron. 119, 176–181.
Zhou, W., Li, K., Wei, Y., Hao, P., Chi, M., Liu, Y., Wu, Y., 2018. Biosens. Bioelectron. 106, 99–104.